One-pot hydrothermal synthesis of BiVO$_4$ microspheres with mixed crystal phase and Sm^{3+}-doped BiVO$_4$ for enhanced photocatalytic activity

Shiwen Zhu[1] •Quanguo Li[1]• Marko Huttula[2]• Taohai Li[1] •Wei Cao[2]

Abstract

The BiVO$_4$ microspheres and Sm^{3+}-doped BiVO$_4$ polygons were prepared through a facile hydrothermal method by using K$_6$V$_{10}$O$_{28}$·9H$_2$O as a novel vanadium source. Optimized temperature and pH value of preparing BiVO$_4$ were obtained. The polycrystalline BiVO$_4$ microspheres prepared at T=140°C, pH=4 demonstrates the best photocatalytic activities for degrading dyes under UV radiation. This is due to transfers of photogenerated electrons from tetragonal to monoclinic phases. In contrast to undoped BiVO$_4$, the photocatalytic activity of Sm^{3+} doped BiVO$_4$ polygons is drastically enhanced not only under UV radiation but also under visible light radiation. An optimized Sm content was found to be 10%. Enhanced efficiency with the doped sample is attributed to the dopants' role inblocking recombination of photogenerated electron-hole pairs. This work offers a simple route to obtain mixed phase BiVO$_4$ and provide an effective way to reach higher photocatalytic activity by doping the Sm^{3+} in the semiconductor catalysts.

Taohai Li(✉)T. Li e-mail: hnlth@xtu.edu.cn

[1]College of Chemistry, Key Lab of Environment Friendly Chemistry and Application in Ministry of Education, Xiangtan University, Xiangtan, 411105, China

[2]Nano and Molecular Materials Research Unit, Faculty of Science,University of Oulu, P.O. Box 3000, FIN-90014, Finland

Introduction

Development of novel and more efficient photocatalysts for degradation of organic contaminants and water splitting has been a key focus of researches in last decades [1-7]. In this sense, Bismuth vanadate ($BiVO_4$) is considered to be one of the promising photocatalysts not only for its interesting technological properties [8], but also for its narrow band gap (2.4 eV) and low toxicity[9-11]. In general, there are many factors which affect the photocatalytic activity of the photocatalysts. Among them, crystal phase and morphology normally dominate. On one hand, crystal phase is a key factor to influence the catalytic properties of the semiconductive catalysts. As for $BiVO_4$, it has three main crystalline phases: monoclinic scheelite, tetragonal zircon and tetragonal scheelite [12-14]. In the past few decades, the researches of $BiVO_4$ mainly focused on $BiVO_4$ with pure phase [15-18]. However, recently, S. Obregón and G. Colón reported on the synthesis of mixed phases of $BiVO_4$ [19-21]. It was further shown by these reports that the mixed phases of $BiVO_4$ can increase the photocatalytic efficiencies in contrast to $BiVO_4$ with pure phase. The improved photocatalytic efficiency is attributed to the promotion of charge separation. On the basis of these frameworks, we attempted to prepare $BiVO_4$ photocatalyst with mixed phase. On another hand, morphology is also a crucial factor which depends on the catalytic properties of the semiconductive catalysts. In recent years, $BiVO_4$ has been synthesized to many 3D architectures such as peanut-shaped nanostructure [22], pillar-like morphology [23], nanosheet [13], nano-leaf [24]

etc. Among these morphologies, the submicron-scale spheres of $BiVO_4$ were found to be distinctive photocatalyst due to its high porousity of the structures, large specific surface area and low band gap energy. And in our recent works, we have successfully synthesized monoclinic $BiVO_4$ nanospheres at 180^oC [25]. These monoclinic $BiVO_4$ nanospheres can degrade RhB effectively under UV light. However, the hydrothermal temperature of preparing $BiVO_4$ nanospheres is still high. Thus, we tried to synthesize $BiVO_4$ with uniform morphology under lower temperature.

Although there are large amount of reports on $BiVO_4$, the photocatalytic activity of the pure $BiVO_4$ are still a bit low because of difficult migration and separation of electron-hole pairs [26-28]. To solve this problem, tremendous efforts have been made to improve the photocatalytic abilities of $BiVO_4$. For example, impurity doping [29-31] and coupling $BiVO_4$ with other semiconductors [19, 32, 33] have been proved as effective ways to enhance catalytic robustness. Among these methods, element doping is considered as an effective way to improve the photocatalytic activity of $BiVO_4$. And in our latest work, the Ag^+-doped $BiVO_4$ was reported to possess enhanced photocatalytic activity in contrast to the pure counterpart [34]. However, the doping of Ag^+ has only little effect on the morphology of $BiVO_4$ and the obtained $Ag^+/BiVO_4$ showed low photocatalytic activity under visible light. Therefore, we attempt to dope $BiVO_4$ with other element in order to improve its photocatalytic activity not only under UV light but also under visible light. In the past few years,

doping BiVO$_4$ with rare earth (RE) elements is regarded as a new way to enhance the photocatalytic activity of the semiconductor [35]. It has been demonstrated that BiVO$_4$ doped by Er^{3+} shows much higher photocatalytic activity [19]. Within a similar strategy, Obregón et al. reported that BiVO$_4$ by Yttrium doping shows improved photocatalytic activity [21].These results clearly show that searching for proper RE dopants will facilitate the design of BiVO$_4$ photocatalytic activities. Within these frameworks, we dope BiVO$_4$ with the rare earth ion Sm^{3+}.

Herein, we have fabricated Sm^{3+}-doped BiVO$_4$ polygonal nanoplates via one-pot hydrothermal method using a novel vanadium source K$_6$V$_{10}$O$_{28}$·9H$_2$O. We studied impacts of synthesis conditions (reaction temperature, initial pH value) on properties of pure BiVO$_4$, and also impacts of doping with different Sm^{3+} contents. The optimized reaction temperature and pH of preparing BiVO$_4$ have been obtained. Besides, after doping BiVO$_4$ with Sm^{3+}, the morphology and photocatalytic activity were improved drastically in contrast to pure BiVO$_4$. A possible photocatalytic mechanism was also proposed. This work may offer an alternative way to achieve higher photocatalytic activity by doping the Sm^{3+} in other semiconductor catalysts.

Materials and methods

Preparation of polycrystalline BiVO$_4$

The BiVO$_4$ photocatalysts were prepared through one-pot solvothermal method under different synthesis conditions. In a typical procedure, Bi(NO$_3$)$_3$·5H$_2$O (4.85 g,

10mmol) and $K_6V_{10}O_{28} \cdot 9H_2O$ (1.29 g, 1mmol) were respectively dissolved in 30 mL

of 2M HNO_3 solution and 30 mL of distilled water at room temperature. Then, the

dissolved $K_6V_{10}O_{28} \cdot 9H_2O$ (V10) solution was added to $Bi(NO_3)_3 \cdot 5H_2O$ solution

dropwise and the mixture was stirred for 1 h to obtain the yellow emulsion. After

tuning the pH of the mixture to a certain value, the suspensions were transferred into

Teflon-lined stainless steel autoclave with a capacity of 100 mL, maintained for 24h at

a certain temperature, and subsequently cooled to room temperature. The bright

yellow precipitate was collected by centrifugation, washed with the deionized water

and ethanol three times, and then dried at 60ºC for 12 h. As shown in Tab.1, the

obtained samples were labeled as BVO-1, BVO-2, BVO-3, BVO-4 according to

reaction conditions. Besides, in order to illustrate the advantage of using the

polyoxometalate V_{10} ($K_6V_{10}O_{28} \cdot 9H_2O$) as the vanadium source, we did comparative

experiment by using the common vanadium source NH_4VO_3. The synthesis process is

identical to the preparation of BVO-1 except for differing the vanadium sources. The

sample prepared by NH_4VO_3 was labeled as BVO-5.

Table1 The reaction conditions for the synthesis of $BiVO_4$.

Sample name	BVO-1	BVO-2	BVO-3	BVO-4	BVO-5
pH value	4	10	4	10	4
Reaction temperature	140ºC	140ºC	160ºC	160ºC	140ºC
Vanadium Source	V_{10}	V_{10}	V_{10}	V_{10}	NH_4VO_3

Preparation of $Sm^{3+}/BiVO_4$ polygons

The synthesis procedure to prepare the Sm^{3+} doped $BiVO_4$ is similar to the one of

pure $BiVO_4$. Only difference is that preset amounts of $SmCl_3 \cdot 6H_2O$ were added into the initial synthesis solution in order to reach different nominal molar ratios of Sm^{3+} in the final products. The initial pH value was adjusted to 4 and the reaction temperature maintained at 160^oC. Detailed feed ratios were listed in Table 2. Products were labeled as S1 (3%), S2 (5%), S3 (7%), S4 (10%) and S5 (15%), respectively.

Table 2 The feed ratio for the synthesis of $Sm^{3+}/BiVO_4$.

ratio	3%	5%	7%	10%	15%
$SmCl_3 \cdot 6H_2O$ (g)	0.0257	0.0428	0.0599	0.0856	0.128

Materials characterization

All of the chemical reagents were analytical purity and without further purification. The crystal structures of the samples were confirmed by X-ray diffraction (XRD, MiniFlex II diffractometer with Cu Kα radiation (λ=0.15406 nm)). The morphology of the as-prepared samples was analyzed by the Scanning Electron Microscopy (SEM, JEOLJSM-6700F). The UV-vis diffuse reflectance spectra were obtained with a UV-visible spectrophotometer (UV-2550, Shi-madzu, Japan). The UV-visible absorption spectra were recorded on a Lambda 25 UV-vis spectrophotometer (Perkin-Elmer, USA) in the range of 400-800 nm. X-ray photoelectron spectroscopy (XPS) measurements were recorded on a PHI 5300 with a monochromatic Mg Kα X-ray as the excitation source to explore the elements on the surface. Binding energy was calibrated with respect to the signal from adventitious C 1s binding energy at 284.8 eV.

Photocatalytic activity measurement

Photocatalytic activities of the samples were evaluated by the degradation of methylene blue (MB) and rhodamine B (RhB) under UV light using a 500W mercury lamp as a light source. Experiments were carried out at room temperature, and steps as follows. Catalysts (50mg) were added to MB (RhB) aqueous solution (10 mg/L, 50 mL) and then magnetically stirred in dark for 30 min before the irradiation. Afterwards, the light source was turned on. During the reaction process, 5 mL of the suspension was taken out at a certain time interval and centrifuged at 3500 rpm for 5 min to remove the photocatalyst completely. The dye concentration of the supernatant was recorded on a Lambda 25 UV-vis spectrophotometer (Perkin-Elmer, USA).

Photocatalytic activities of the Sm-doped $BiVO_4$ under visible light were determined by the degradation of RhB and MB. Typically, the as-prepared photocatalysts (50 mg) were dispersed in RhB (MB/DNP) solution (10 mg/L, 50 mL) and magnetically stirred in dark for 30 minutes before the illumination. Then, the suspension was exposed to a 300 W tungsten halogen lamp under magnetic stirring. A 420 nm cut-off glass filter was installed before the output of the light source in order to eliminate UV light. At 30 min intervals, 5 mL of the suspension were collected and separated by centrifugation to remove the photocatalysts for analysis. Variations in the concentration of RhB (MB/DNP) were recorded using a Lambda 25 UV-vis spectrophotometer.

Scavenging experiments for reactive oxidative species

The scavenging experiment for the reactive species is similar to the photocatalytic degradation process. The role of reactive oxidative species in the photocatalytic

process was evaluated by adding two different scavengers, isopropanol (1mM, OH•

scavenger) and KI (1mM, h^+ scavenger) into the reaction solution (MB) before the

addition of the photocatalyst.

Results and discussion

Microstructures of BiVO$_4$

The effect of the reaction conditions (initial pH value and reaction temperature) on

the phase structures of the obtained BiVO$_4$ was investigated via powder X-ray

diffraction (XRD) measurement. As shown in Fig. 1, the BiVO$_4$ powder prepared at

160°C was in good agreement with the monoclinic phase of BiVO$_4$ of lattice constants

a=0.5195Å, b=1.1701Å and c=0.5092Å (JCPDS NO. 14-0688). No characteristic

peaks of other impurities and undecomposed reactants are observed, demonstrating

high purity of the BiVO$_4$ prepared at 160°C. However, BiVO$_4$ synthesized at 140°C

shows a mixture of monoclinic (JCPDS NO. 14-0688) and tetragonal (JCPDS NO.

14-0133) crystalline phases. From the above analysis, it can be concluded that when

the reaction temperature rises from 140°C to 160°C, the phase structures of the

obtained BiVO$_4$ transform from a mixture phase to monoclinic phase. This is because

the tetragonal phase of BiVO$_4$ can't be formed under high reaction temperature. The

trend was further seen in BiVO$_4$ (prepared at pH=4, T=180°C), which has been

reported before [25]. Prepared at 180°C, BiVO$_4$ has pure monoclinic phase, and no

other characteristic peaks of tetragonal BiVO$_4$ could be detected.

The pH values have an impact on the crystallinity of the product. As shown in

Fig. 1, when the temperature is constant to 140°C, the peak at 18.669^o and 18.988^o

disappeared with the increase of the pH value. Similarly, when the temperature is

constant to 160ºC, the peak at 32.679º and 34.714º disappeared with the increase of the pH value. This indicates the crystallinity of the product prepared at pH=4 is better.
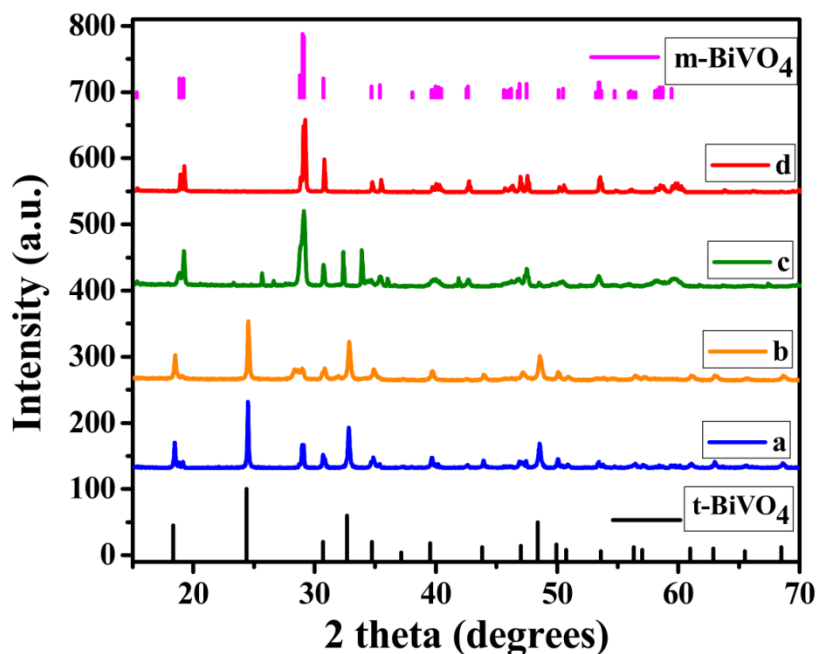

Fig.1 XRD patterns of BiVO$_4$ fabricated at different reaction conditions (a) BVO-1; (b) BVO-2; (c) BVO-3; (d) BVO-4

Morphology of polycrystalline BiVO$_4$

Impacts from the reaction conditions on BiVO$_4$ morphology were investigated by SEM. As shown in Fig. 2a and b, the morphologies of both the BVO-1 and BVO-2 particles are microspheres with the diameters ranging from 2 to 5 μm, suggesting that the obtained polycrystalline BiVO$_4$ showed spherical morphology. The surface of BVO-2 is rougher than BVO-1. Interestingly, there are several tiny flocculent particles distributing around BiVO$_4$ microspheres, which are probably the primary 'building brick' nanoparticles of the BiVO$_4$ shells. The situation is quite different for that of BiVO$_4$ sample prepared at 160ºC. As shown in 2c and d, BVO-3 exhibit rod-like morphology while BVO-4 exhibit irregular plate-like morphology. Some of

the particles of BVO-4 agglomerate. This is probably because $BiVO_4$ microspheres are broken into tiny irregular particles under higher hydrothermal temperature.

It can be concluded from the above results that the initial pH value and the reaction temperature have impacts on morphology and phase structures of the $BiVO_4$.
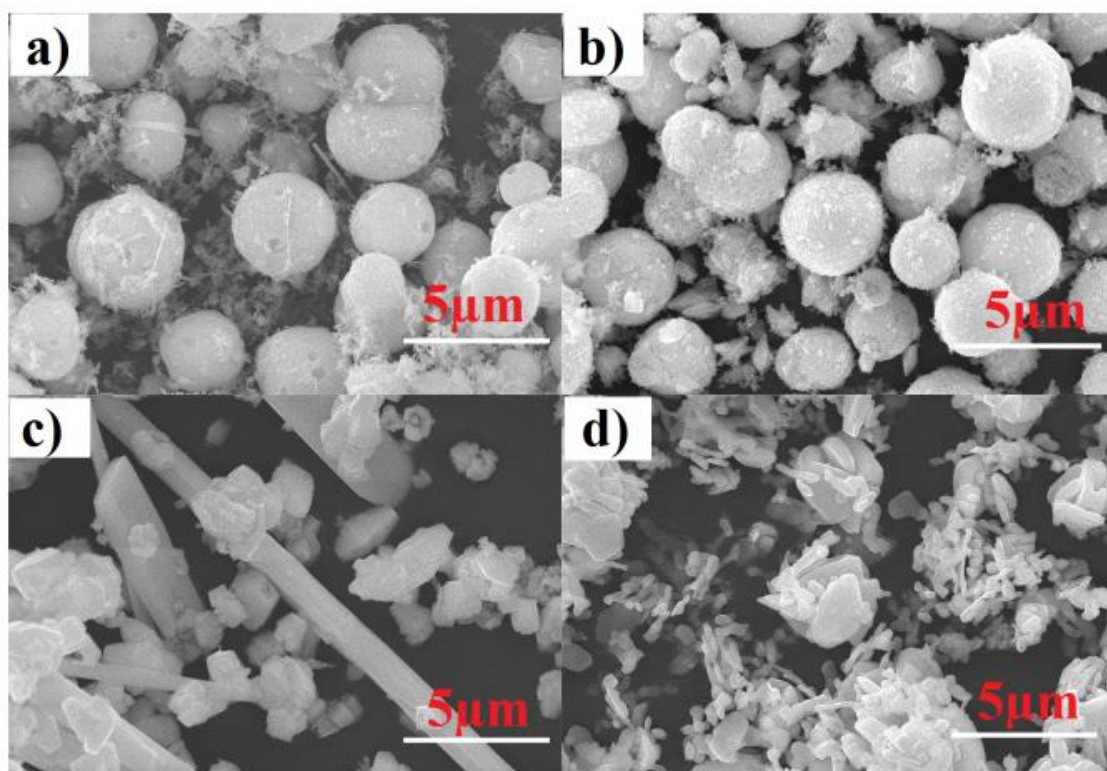

Fig. 2 SEM images of $BiVO_4$ fabricated at different reaction conditions (a) BVO-1; (b) BVO-2; (c) BVO-3; (d) BVO-4

Band gap of polycrystalline $BiVO_4$

Band gap of the semiconductive photocatalysts plays an important role in photocatalytic activity [36]. Here we employed the UV-vis spectroscopy to determine the bandgap and results were depicted in Fig. 3. The absorption edges of $BiVO_4$ were estimated at 514 nm (BVO-1), 509 nm(BVO-2), 517 nm (BVO-3) and 516 nm (BVO-4). Following the formula $Ah\nu = C (h\nu-Eg)1/2$, the band gap (Eg) of $BiVO_4$

was calculated to 2.41eV (BVO-1), 2.48eV (BVO-2), 2.39eV (BVO-3) and 2.39eV (BVO-4), respectively. In the optical transition, photoexcited electrons were prompted from valence bands (VB) consisting of O 2p into the conduction bands (CB) of V 3d orbitals [37]. Additionally, under the same reaction temperature, the samples exhibit slight blue-shift of their absorption edges as the pH value increases. This is because the initial pH will distort the VO_4^{3-} tetrahedron[38], resulting in a slight difference in the electronic structure of the samples.
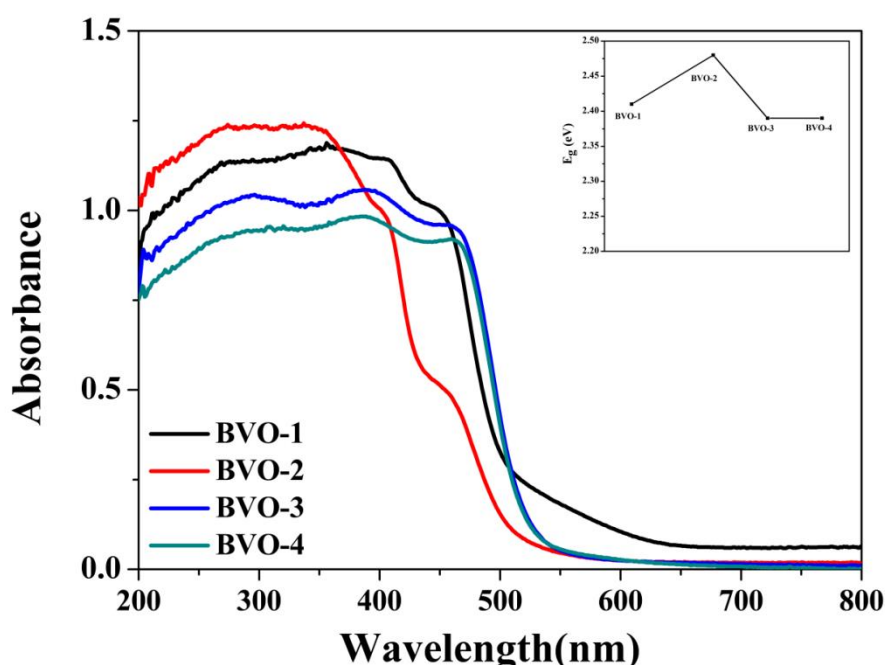
Fig.3 UV-vis diffuse reflectance spectra of $BiVO_4$ fabricated at different reaction conditions (a) BVO-1; (b) BVO-2; (c) BVO-3; (d) BVO-4

Photocatalytic activity of polycrystalline BiVO₄

The photocatalytic activities of $BiVO_4$ samples obtained at different reaction conditions were measured via degradation of RhB and MB aqueous solutions under UV light illumination. The UV-vis spectra which was taken over time during the photodegradation of RhB are shown in Figure 4. From Fig.4a that BVO-1 and BVO-2 leads to higher photoactivity for degrading of RhB with respect to BVO-3 and BVO-4. After irradiation for 150min, the removal rate of RhB concentration is 94.74%,

89.47%, 82.11% and 88.42% for BVO-1, BVO-2, BVO-3 and BVO-4 respectively. This implies that the appearance of the tetragonal phase can enhance the photocatalytic activity of systems. Such a claim is further proved by comparing the present results with the one reported for $BiVO_4$ (prepared at pH=4, T=180°C). In a previous study [25], after 150min irradiation, the photodegradation rate of RhB concentration was found 84.1% for $BiVO_4$ (prepared at pH=4, T=180°C). Thus, BVO-1 has better photocatalytic performance to degrade RhB than any other samples, including $BiVO_4$ (prepared at pH=4, T=180°C) studied in the previous work. The photocatalytic degradation kinetics of RhB was studied in order to quantitative compare the photocatalytic activities of as-prepared samples. The photodegradation kinetics of RhB was shown in Fig.4b. It is seen that the degradation rate of BVO-1 is bigger than these of other samples. It can be concluded that $BiVO_4$ fabricated at lower temperature exhibited superior photocatalytic activity.
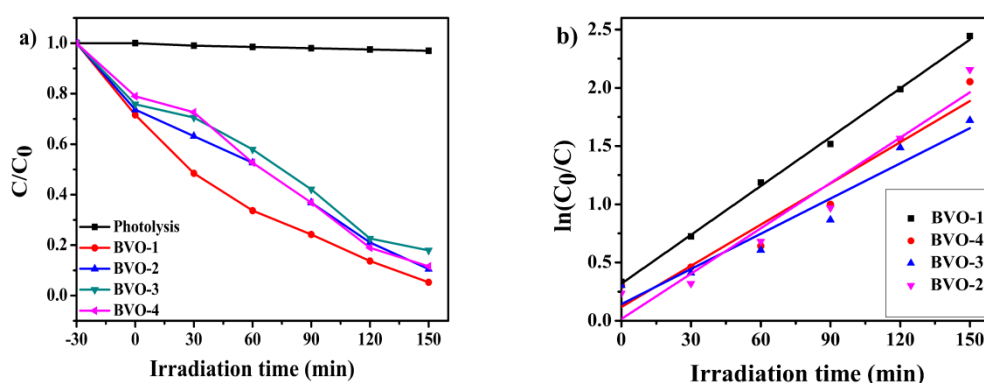

Ｆｉｇ. 4 Time-course variation of (a) C/C_0 and (b) $\ln(C_0/C)$ of RhB solution under UV light irradiation in the presence of BVO-1, BVO-2, BVO-3 and BVO-4 as the photocatalyst

It is worth noting that BVO-1 and BVO-2 also results in higher photocatalytic performance for degrading of MB in contrast to BVO-3 and BVO-4 (Fig. 5). Thus the optimum conversion value is achieved by $BiVO_4$ (140°C, pH=4). For BVO-1, the complete MB degradation is achieved after 90 min of illumination. As show in Fig.5b,

the reaction rate for BVO-1 is approximately 5 times higher than BVO-3. These results imply that BVO-1 has the best photocatalytic activity to degrade dyes among all samples.
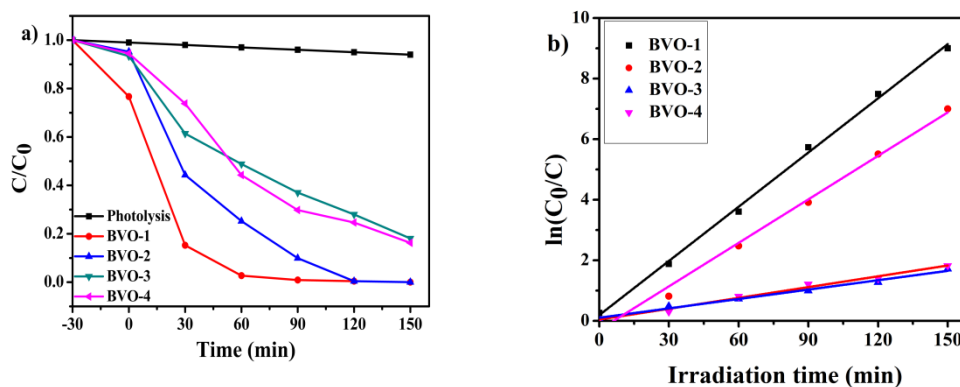

F i g. 5 Time-course variation of (a) C/C_0 and (b) $\ln(C_0/C)$ of MB solution under UV light irradiation in the presence of BVO-1, BVO-2, BVO-3 and BVO-4 as the photocatalyst

Photocatalytic mechanism

A possible mechanism of the photocatalytic degradation process in the mixed phase of $BiVO_4$ (m-$BiVO_4$/t-$BiVO_4$) was illustrated in Fig. 6. Interface junction was formed between the t-$BiVO_4$ and m-$BiVO_4$. The energy of UV light is enough to excite the valence band (VB) electrons of both t-$BiVO_4$ and m-$BiVO_4$ to the conduction band (CB). Then, the light-induced conduction band electrons in m-$BiVO_4$ were quickly transferred to the conduction band of t-$BiVO_4$ and the valence band holes in t-$BiVO_4$ were transferred to the valence band of m-$BiVO_4$. This promoted the separation of e^--h^+ and is beneficial to the photocatalytic activity of $BiVO_4$.
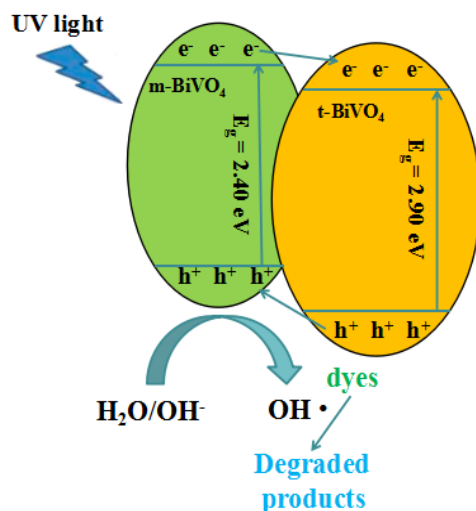
13

Fig. 6 The possible mechanism of the photocatalytic reaction in m-BiVO$_4$/t-BiVO$_4$

Impacts of different vanadium sources

In order to illustrate the advantage of using the polyoxometalate K$_6$V$_{10}$O$_{28}$·9H$_2$O as the vanadium source, we did comparative experiment by using the common vanadium source NH$_4$VO$_3$. As shown in Fig. 7a, BiVO$_4$ fabricated by using NH$_4$VO$_3$ as vanadium source also shows a mixture of monoclinic (JCPDS NO. 14-0688) and tetragonal (JCPDS NO. 14-0133) crystalline phases. However, the peak of (110) plane and (011) plane at 18.669° and 18.988°, indexed to monoclinic BiVO$_4$, appeared when K$_6$V$_{10}$O$_{28}$·9H$_2$O is used as vanadium source. This indicates that the crystallinity of BVO-1 is better than BVO-5.

Fig. 7b shows the morphology of BiVO$_4$ fabricated by using different vanadium source. It is obviously that BVO-5 shows spherical shape. However, in contrast to BVO-5, BVO-1 is rounder and the surface of BVO-1 is smoother.
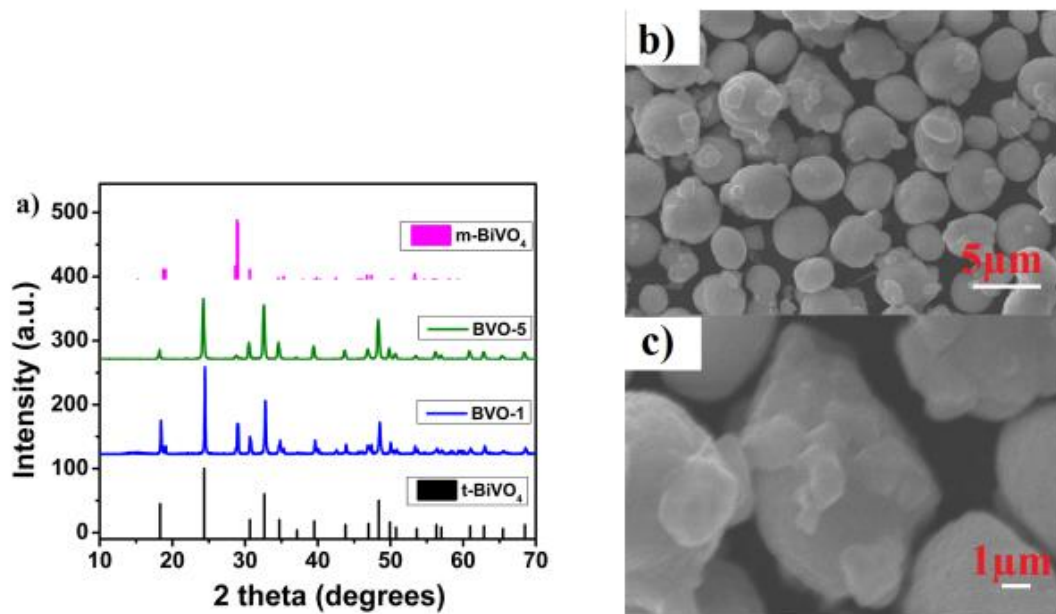
Ｆｉｇ. 7 (a) XRD patterns of $BiVO_4$ fabricated by using different vanadium source; (b)(c) SEM images of BVO-5

The photocatalytic performance of $BiVO_4$ fabricated by using different vanadium source was evaluated by degradation of MB under UV light. As shown in Fig. 8, the removal rate of MB in the presence of the $BiVO_4$ fabricated by NH_4VO_3 is only 55.6% in 150 min. However, as for $BiVO_4$ fabricated by $K_6V_{10}O_{28}\cdot 9H_2O$ sample, nearly all of MB can be degraded in 90min.
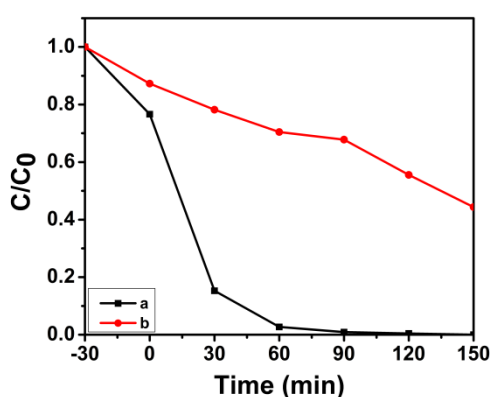
Ｆｉｇ. 8 Time-course variation of C/C_0 of MB solution under UV light irradiation in the presence of $BiVO_4$ fabricated by using different vanadium source: (a) $K_6V_{10}O_{28}\cdot 9H_2O$; (b) NH_4VO_3.

In a word, different vanadium source can result in the different properties of the

product. The morphology of BVO-1 is rounder than that fabricated by BVO-5. Besides, BVO-1 exhibits much higher photocatalytic activity than BVO-5.

The advantage of using $K_6V_{10}O_{28} \cdot 9H_2O$ can be illustrated not only by the above experimental data, but also can be illustrated as follows: As is known to us, in the case of strong acid, H^+ can makes condensation of VO_3^- and results in the formation of isopolyacid salt such as $V_{10}O_{28}^{6-}$. However, $K_6V_{10}O_{28} \cdot 9H_2O$ can still exist in strong acid. That is to say, we can fabricate $BiVO_4$ in a wide pH range if using $K_6V_{10}O_{28} \cdot 9H_2O$ as vanadium source.

From the above results, it can be concluded that BVO-1 has the best morphology and photocatalytic activity than other samples. This is probably because mixed phase of $BiVO_4$ is beneficial to promote the separation of e^--h^+. Thus, the optimum reaction hydrothermal condition of preparing $BiVO_4$ is obtained. Besides, in order to improve the morphology and photocatalytic activity of BVO-3, we dope it with Sm^{3+}.

However, it should be noted that the as-prepared $BiVO_4$ microspheres with mixed phases can only exhibit photocatalytic activity under UV light irradiation. This drastically limits a wider applicable scopes of the photocatalyst under other conditions, e.g., the visible light irridation. Therefore, future studies may be concentrated on further solving this problem by coupling with the other suitable semiconductors.

The doping effect of Sm^{3+} on $BiVO_4$

Microstructures of Sm^{3+} doped $BiVO_4$

The XRD diffraction patterns of the $Sm^{3+}/BiVO_4$ samples with different Sm^{3+} contents are shown in Fig. 9. The crystal phases of Sm-doped $BiVO_4$ is broadly similar to the pure $BiVO_4$. It can be seen that the synthesized samples were in good

agreement with the monoclinic phase of $BiVO_4$ (JCPDS NO. 14-0688). From the microstructural determinations, the diffraction peak intensity of (200) plane, which can be indexed as tetragonal $BiVO_4$, gradually decreasing with the content of Sm^{3+} increasing. This is probably because the appearance of Sm^{3+} can inhibit the growth of the (200) plane. In addition, the (114) crystal plane of Sm (JCPDS NO. 37-1446) was observed after the doping of Sm, suggesting that Sm was successfully doped in $BiVO_4$. Moreover, with the content of Sm^{3+} increasing from 3% to 15%, the (114) peak intensity at 60.1º slightly increased, indicating that larger contents of Sm in the product. Besides, no impurity peaks are observed, suggesting that the obtained products were in high purity. It is also shown that there are no diffraction peaks of SmO or other compounds containing Sm.
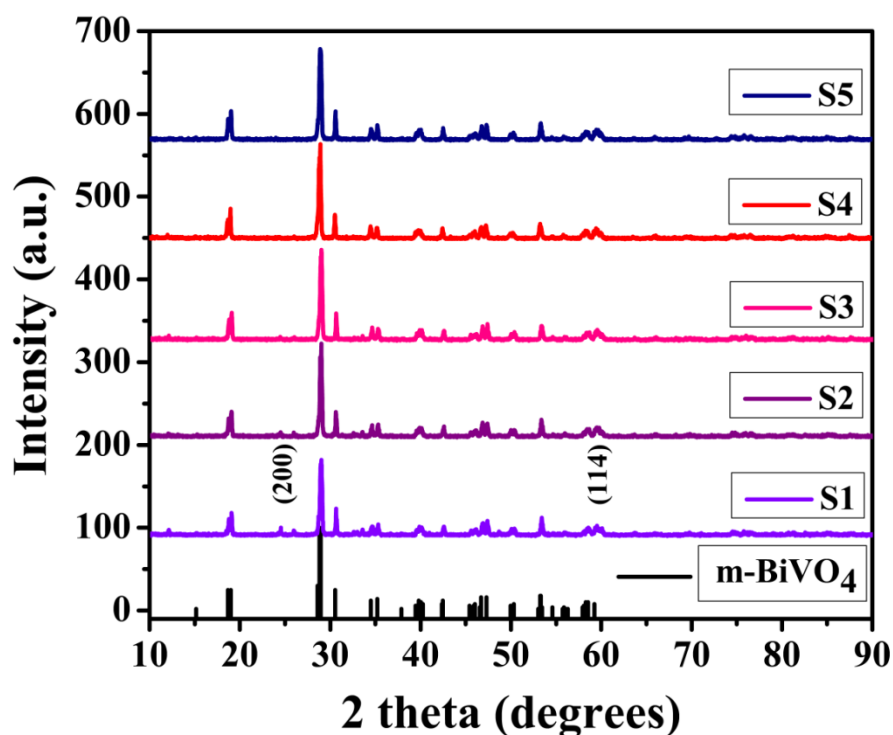

Ｆｉｇ. 9 XRD patterns of the products with different molar ratios of Sm^{3+} to $BiVO_4$

X-ray photoelectron spectral determination

Fig. 10a shows that the Sm^{3+}-doped $BiVO_4$ is composed of Bi, V, O, Sm and C. The C element is ascribed to the adventitious hydrocarbon from XPS instrument itself. Fig. 10c shows the high-resolution XPS spectrum of the Bi 4f. The peaks with binding energy of 158.6 and 163.9 eV are from Bi 4f7/2 and Bi 4f5/2 of Bi^{3+} in $BiVO_4$[39]. The XPS spectrum of V $2p^3$ is shown in Fig. 10d. The peaks around 524 eV and 516 eV denote at binding energies of V2p1/2 and V2p3/2 in the pure $BiVO_4$. Chemical state of V in the sample is +5 valence[40]. The Sm associated peaks in Fig. 10f at binding energies of around 1081 eV correspond to the Sm^{3+} ion[41], suggesting that Sm ions existed as Sm^{3+} in the samples.
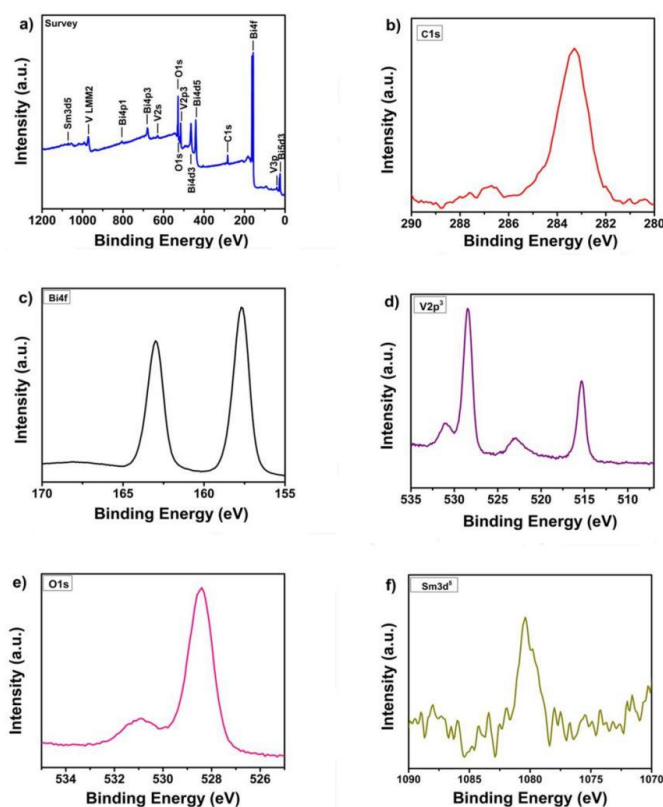

Fig. 10 XPS spectra of Sm^{3+}-doped $BiVO_4$: (a) XPS survey spectrum; (b) XPS spectrum of C 1s; (c) XPS spectrum of Bi 4f; (d) XPS spectrum of V2p^3; (e) XPS spectrum of O1s; (f) XPS spectrum of Sm 3d^5

Morphologies of Sm^{3+} doped $BiVO_4$

The SEM images of $Sm^{3+}/BiVO_4$ are shown in Fig. 11. All of the Sm^{3+}-doped $BiVO_4$ particles are dispersed uniformly. It is clear seen that there are a significant distinction between pure $BiVO_4$ and Sm doped $BiVO_4$. Pure $BiVO_4$ (BVO-3) shows irregular shape while the morphology of Sm doped systems was similar to the polygons. The probably explanation for this phenomenon is that Sm^{3+} plays an important role in guiding the directional growth of the nanoparticles during the secondary aggregates. Moreover, with the increase of Sm^{3+}doping content, the average particle size of $Sm^{3+}/BiVO_4$ catalysts seem to be larger and the morphology transit from irregular polygons to approximation of round-like shape, indicating that the doping content of Sm has an effect on the morphology of $BiVO_4$. From the above results, the size and morphology of $BiVO_4$ can be controlled by adjusting the doping content of Sm^{3+}. This is different from doping of Ag^+into $BiVO_4$, where no effort on the $BiVO_4$ were changed after doping [34].
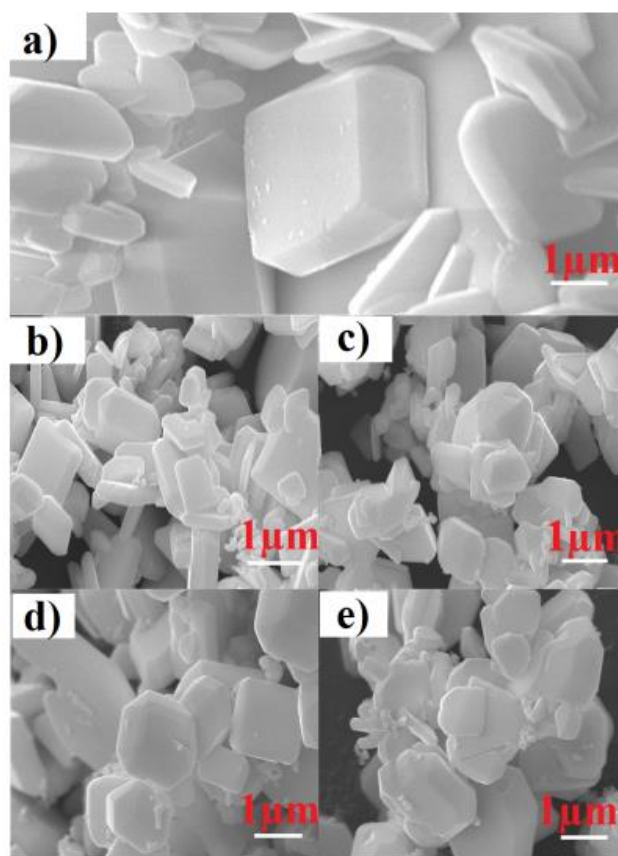
Band gap of Sm^{3+} doped $BiVO_4$

Fig. 12 shows the UV–vis diffuse reflectance spectra (DRS) spectra of Sm^{3+}-doped $BiVO_4$ composites in contrast to pure $BiVO_4$. The absorption spectrum of 10% Sm^{3+}-doped $BiVO_4$ sample is stronger and broader in visible region. This is probably due to additional transition channels from d-like orbits in the VBs to the additional samarium f-like orbits in the CBs, which is resulted from the partially-filled atomic f shell of Sm. However, the absorption spectrum of 10% Sm^{3+}-doped $BiVO_4$ is weaker in ultraviolet region. As shown in Fig.12, the absorption edge of Sm^{3+}-doped $BiVO_4$ is 663 nm. The band gap energy (Eg) of the Sm-doped $BiVO_4$ can be estimated

according to the formula $Ah\nu = C(h\nu - E_g)^{1/2}$, and founded to be about 1.870eV, which is much narrower than that of pure $BiVO_4$. In a word, the absorption of light for Sm^{3+}-doped $BiVO_4$ photocatalyst is obviously enhanced under visible light and the E_g of Sm-doped $BiVO_4$ is narrower in contrast to pure $BiVO_4$, which potentially inhibits the recombination rate of electron-hole pairs of $BiVO_4$, leading to the enhanced photocatalytic performance under visible light.
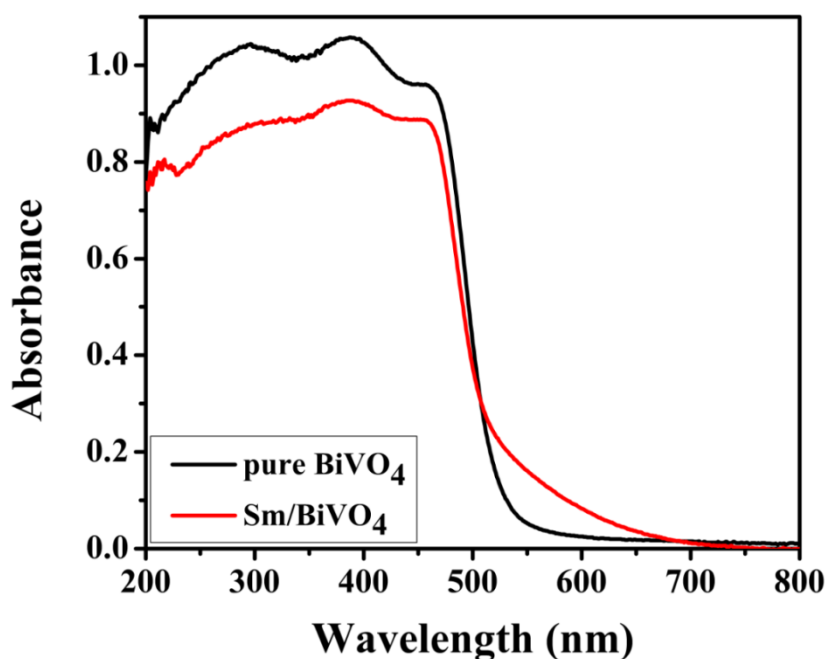

Fig. 12 UV-vis diffuse reflectance spectra of pure $BiVO_4$ and Sm^{3+}-doped $BiVO_4$

Photocatalytic activity under UV light irradiation of Sm^{3+} doped $BiVO_4$

Photocatalytic activity of the doped products was measured by degradation of MB (RhB) solution (10 mg/L) under UV light. Change of the RhB concentrations was depicted in Fig. 13. The photolysis test (solid line in Fig. 13a) shows no obvious change in the concentration of RhB, illustrating that the self-degradation of RhB is extraordinarily slow and negligible under UV light illumination. In Fig.13a,

Sm^{3+}/BiVO$_4$ has an enhanced photocatalytic degradation for RhB in contrast to BVO-3, suggesting that the doping of Sm^{3+} can improve the photocatalytic activity of BiVO$_4$ for degrading RhB. Furthermore, with an increase in the doping content of Sm^{3+}, it can be seen that the photocatalytic degradation rate of BiVO$_4$ increases to a certain value and then decreases. The photodegradation rate of sample S4 is the highest and RhB is degraded completely after 150 min. Fig. 13b shows the pseudo-first-order reaction kinetics of BiVO$_4$ doped with different content of Sm^{3+}. The rate constant values of RhB degradation are 0.0074 min^{-1}, 0.0080 min^{-1}, 0.0133 min^{-1}, 0.0254 min^{-1} and 0.0191 min^{-1} for S1, S2, S3, S4 and S5, respectively. From the above results, we found the degradation rate of S4 is faster than other samples, suggesting that sample S4 has the best photocatalytic activity to degrade RhB.
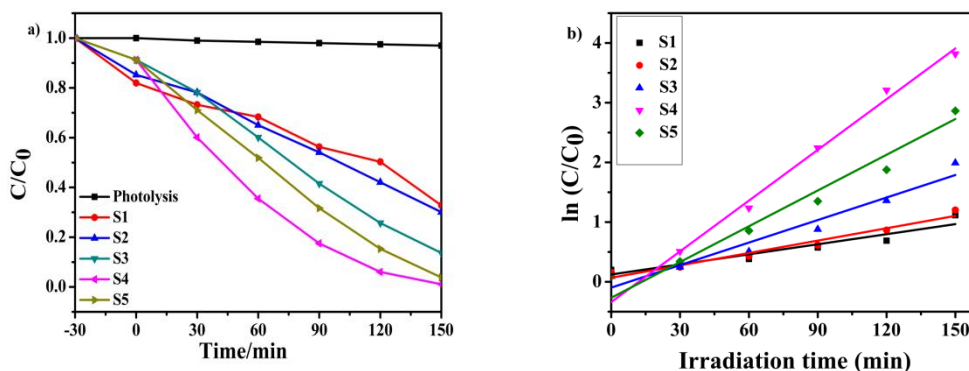

F i g. 13 Time-course variation of (a) C/C$_0$ and (b) ln(C$_0$/C) of RhB solution under UV light irradiation in the presence of S1, S2, S3, S4 and S5 as the photocatalyst

Fig. 14a shows photocatalytic results of the obtained Sm^{3+}/BiVO$_4$ photocatalysts for MB. The photocatalytic efficiency of the samples (S1, S2, S3, S4 and S5) have achieved approximately 99% after 150 min UV irradiation. The degradation efficiency of MB for S1, S2, S3, S4 and S5 are 76%, 76%, 86%, 95% and 76% for 60

min, respectively. The photocatalytic degradation kinetics of MB are show in Fig. 14b. It is observed that the degradation rate of S4 is faster than other sample. From the RhB and MB catalytic tests, sample S4 is found to possess the best photocatalytic activity to degrade dyes. An optimum Sm doping content of 10% is found.
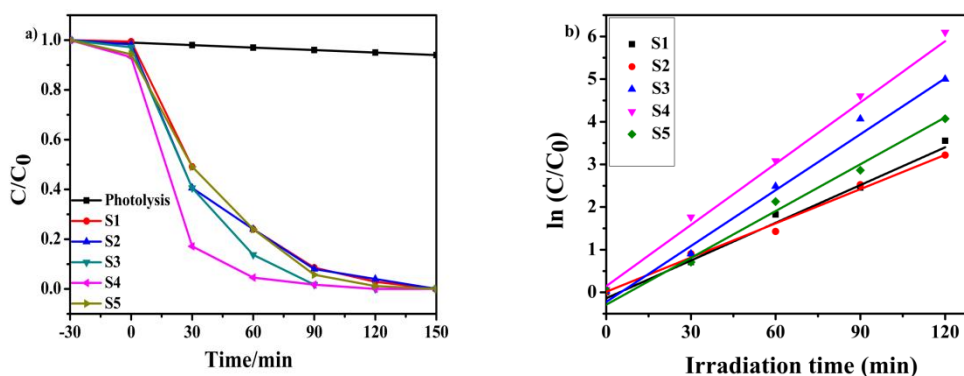

Fig. 14 Time-course variation of (a) C/C_0 and (b) $\ln(C_0/C)$ of MB solution under UV light irradiation in the presence of S1, S2, S3, S4 and S5 as the photocatalyst

To further evaluate photocatalytic efficiency of Sm^{3+}-doped $BiVO_4$, we compare the results from doped $BiVO_4$ with pure $BiVO_4$ (BVO-3) under the same conditions. Fig. 15 shows the photocatalytic performances of pure and Sm-doped $BiVO_4$. The results show that the degradation rate of MB for pure and Sm^{3+}-doped $BiVO_4$ are 55% and 84% for 30 min, respectively. As for RhB dyes, the degradation rate for pure and Sm^{3+}-doped $BiVO_4$ are 57% and 82% for 90 min. Thus, the Sm-doped $BiVO_4$ samples exhibit higher degradation efficiency than pure $BiVO_4$, indicating that doping rare earth ion Sm^{3+} can effectively improves the photocatalytic activities of $BiVO_4$.
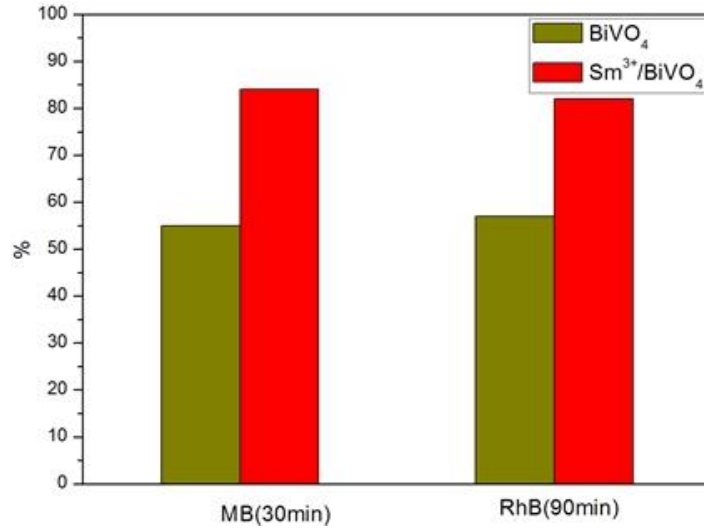
Ｆｉｇ.15 The degradation rate of different dyes under UV light illumination over pure BiVO$_4$ and 10% Sm^{3+}/BiVO$_4$

Photocatalytic activity under visible light irradiation

Photocatalytic activity of the prepared samples under visible light illumination were evaluated by degradation of MB (RhB/DNP), as shown in Fig. 16. It is clearly shown that 10% Sm^{3+}-doped BiVO$_4$ achieved degradation efficiency of 95.31%, 97.71%, and 55.25% for degradation of MB, RhB and DNP respectively under identical reaction for 180 min. This indicates the excellent visible light photocatalytic performance of the obtained samples due to the promoted photogenerated charge separation. And the photocatalytic activity of Sm^{3+}-doped BiVO$_4$ is better than Ag$^+$-doped BiVO$_4$[34] under visible light. This is due to dopant'scontributions to the VB densities of states. In the present case, the partially-filled atomic f shell of Sm[42] can offer more unoccupied vacancies in the VB than the entirely-filled shells from the Ag$^+$.
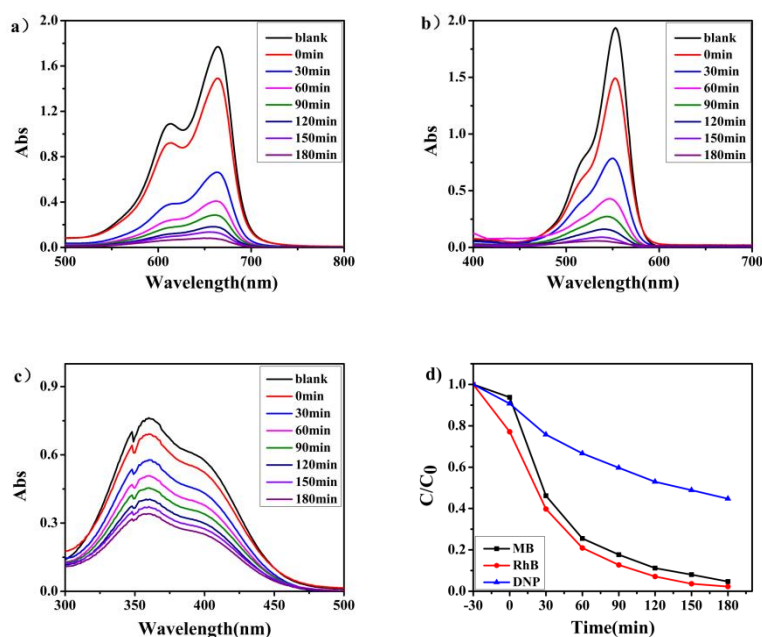
24

Ｆｉｇ.16 UV-Vis absorption spectrum of the (a)MB; (b)RhB; (c)DNP solution (10 mg/L) in the presence of the 10%Sm-doped $BiVO_4$ under visible light illumination. (d) Time-course variation of C/C_0 of the dyes under visible light illumination over 10%Sm-doped $BiVO_4$

Photocatalytic mechanism

The radicals and holes trapping experiments have been performed to investigate the photocatalytic degradation process by 10%Sm^{3+}/$BiVO_4$, in which KI (1mM) and IPA (Isopropanol, 1mM) are used as the hole and OH· scavengers, respectively. As observed from Fig. 17, the photocatalytic activity of 10%Sm^{3+}/$BiVO_4$ decreases slightly after adding KI, suggesting the least importance of h^+ in the photocatalytic process. However, a noticeable inhibition in the photocatalytic degradation efficiency was observed in the presence of IPA. It is obvious from the above results that OH· are the major active species to oxidize MB dye.
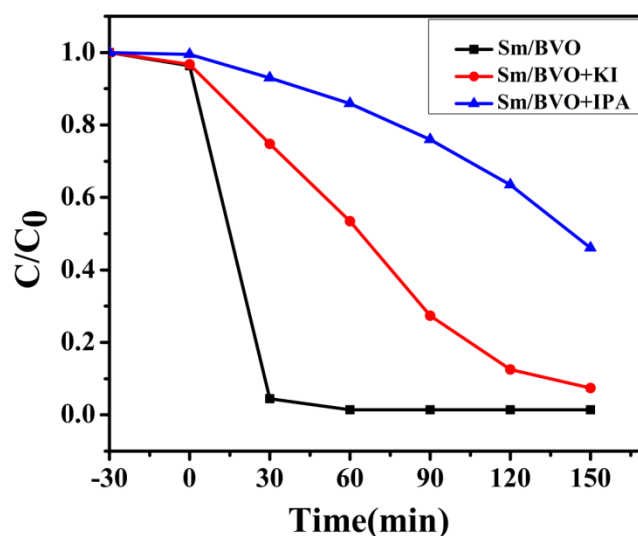
Ｆｉｇ. 17 Photodegradation of MB over the obtained 10%Sm/BiVO$_4$ in the presence of

different scavengers.

According to the above results, a possible photocatalytic mechanism is proposed

and illustrated in Fig. 18. The energy of visible light is enough to promote the VB

electrons of BiVO$_4$ to CBs. Then, Sm^{3+} is immediately reduced into Sm by capturing

the photoexcited electron because of large electronegativity of the Sm^{3+} and the

partially filled f shell. Thus, the photogenerated charges separation can be effectively

promoted, which is beneficial for enhancing the photocatalytic activity of BiVO$_4$.

Besides, the presence of Sm^{3+} resulted in a new electronic transition from the valence

band of BiVO$_4$ to the empty Sm^{3+}/Sm energy levels which is known as a sub-band

gap[42]. This accelerate the separation of e$^-$-h$^+$ pairs. The remained holes in the

valence band of BiVO$_4$ can react with water to form OH·. These reactive OH· species

can oxidize organic dye effectively.

In all, the doping of Sm can prevent the recombination of light-induced e$^-$-h$^+$ pairs

because Sm can capture e^- and quickly transfer to lower charged states with the electrons. The generation of OH· and the high separation rate of the photogenerated charges play an important role in enhancing the photocatalytic activity of $BiVO_4$.

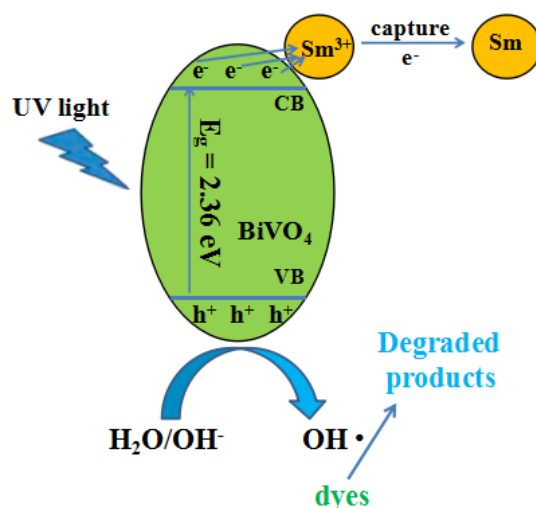Fig. 18 The proposed mechanism of the photocatalytic reaction in $10\%Sm^{3+}/BiVO_4$

Conclusion

In summary, the $BiVO_4$ microspheres with mixed crystal phase was successfully fabricated by a facial one-pot hydrothermal method. The results show that $BiVO_4$ with mixed crystal phase shows high photocatalytic activity towards MB and RhB photodegradation, much better than tetragonal $BiVO_4$. This is probably ascribed to the existence of tetragonal phase. Following the high removal efficiency of RhB and MB exhibited in this study, $BiVO_4$ with mixed crystal phase can be considered as a promising photocatalyst for decolorizing the dyes from wastewater. Moreover, we doped tetragonal $BiVO_4$ with Sm^{3+} in order to tune product morphology and photocatalytic activity. The SEM revealed that the morphology of tetragonal $BiVO_4$

has been improved and the Sm^{3+}-doped $BiVO_4$ were uniform polygons. Furthermore, the obtained Sm^{3+}-doped $BiVO_4$ photocatalyst could degrade RhB and MB more effectively under UV light and visible light irradiation compared to pure $BiVO_4$. This was because the existence of Sm^{3+} could promote the separation of photogenerated electron-hole pairs by capturing the light-induced electrons.

Acknowledgments

References

[1] A.P. Zhang, J.Z. Zhang (2010) Synthesis and characterization of $Ag/BiVO_4$ composite photocatalyst, Appl Surf Sci 256:3224.

[2] J.G. Qu, N.N.Li, B.J.Liu et al (2013) Preparation of $BiVO_4$/bentonite catalysts and their photocatalytic properties under simulated solar irradiation, Mat Sci Semicon Proc 16:99.

[3] K.L. Zhang, C.M. Liu, F.Q. Huang et al (2006) Study of the electronic structure and photocatalytic activity of the BiOCl photocatalyst, Appl Catal B Environ68:125.

[4] Z.B. Zhang, C.C. Wang, R. Zakaria et al (1998) Role of Particle Size in Nanocrystalline TiO$_2$-Based Photocatalysts, J Phys Chem B 102:10871.

[5] C.Y. Yang, F. Li, T.H. Li et al (2016) Ionic-liquid assisted ultrasonic synthesis of BiOCl with controllable morphology and enhanced visible light and sunlight photocatalytic activity, J Mol Catal A Chem 418:132-137.

[6] T.H. Li, S.Y. Gao, F. Li et al (2009) Photocatalytic property of a keggin-type polyoxometalates-containing bilayer system for degradation organic dye model, J Colloid Interf Sci 338:500-505.

[7] Y. Chen, F. Li, W. Cao, T.H. Li (2015) Preparation of recyclable CdS photocatalytic and superhydrophobic films with photostability by using a screen-printing technique, J Mater Chem A 3:16934-16940.

[8] A.P. Zhang, J.Z. Zhang (2010) Effects of europium doping on the photocatalytic behavior of BiVO$_4$, J Hazard Mater 173:265.

[9] S. Kunduz, G.S.P. Soylu (2015) Highly active BiVO$_4$ nanoparticles: The enhanced photocatalytic properties under natural sunlight for removal of phenol from wastewater, Sep Purif Technol 141:221.

[10] Y. Lu, Y.S. Luo, D.Z. Kong et al (2012) Large-scale controllable synthesis of dumbbell-like BiVO$_4$ photocatalysts with enhanced visible-light photocatalytic activity, J Solid State Chem 186:255.

[11] U.M. García-Pérez, A.Martínez-de la Cruz, S.Sepúlveda-Guzmán et al (2014)

Low-temperature synthesis of $BiVO_4$ powders by Pluronic-assisted hydrothermal method: Effect of the surfactant and temperature on the morphology and structural control, Ceram Int 40:4631.

[12] S. M. Thalluri, S. Hernández, S. Bensaid et al (2016) Green-synthesized W- and Mo-doped $BiVO_4$ oriented along the {040} facet with enhanced activity for the sun-driven water oxidation, Appl Catal B Environ180:630.

[13] L. Zhang, D.R. Chen, X.L. Jiao (2006) Monoclinic Structured $BiVO_4$ Nanosheets: Hydrothermal Preparation, Formation Mechanism, and Coloristic and Photocatalytic Properties, J Phys Chem B 110:2668.

[14] D.N. Ke, T.Y. Peng, L. Ma et al (2008) Photocatalytic water splitting for O_2 production under visible-light irradiation on $BiVO_4$ nanoparticles in different sacrificial reagent solutions, Appl Catal A Gen 350:111.

[15] W.Z. Yin, W.Z. Wang, L. Zhou et al (2010) CTAB-assisted synthesis of monoclinic $BiVO_4$ photocatalyst and its highly efficient degradation of organic dye under visible-light irradiation, J Hazard Mater 173: 194-199.

[16] H.M. Fan, D.J. Wang, L.L. Wang et al (2011) Hydrothermal synthesis and photoelectric properties of $BiVO_4$ with different morphologies: An efficient visible-light photocatalyst, Appl Surf Sci 257: 7758-7762.

[17] H.M. Yuan, J.L. Liu, J. Li et al (2015) Designed synthesis of a novel $BiVO_4$-Cu_2O-TiO2 as an efficient visible-light-responding photocatalyst, J Colloid Interf Sci 44: 58-66.

[18] U. Lamdab, K. Wetchakun, S. Phanichphant et al (2015) Highly efficient visible light-induced photocatalytic degradation of methylene blue over $InVO_4$/$BiVO_4$

composite photocatalyst, J Mater Sci (2015) 50: 5788-5798.

[19] S. Obregón, G. Colón (2014) Heterostructured Er^{3+}doped BiVO$_4$with exceptional photocatalytic performance by cooperative electronic and luminescence sensitization mechanism, ApplCatalB Environ 158-159:242-249.

[20] S. Obregón, G. Colón (2014) Excellent photocatalytic activity of Yb^{3+}, Er^{3+}co-doped BiVO$_4$ photocatalyst, Appl Catal B Environ152-153:328-334.

[21] S. Usai, S. Obregón, A.I. Becerro, G. Colón (2013) Monoclinic-Tetragonal Heterostructured BiVO$_4$ by Yttrium Doping with Improved Photocatalytic Activity, J Phys Chem C 117:24479-24484.

[22] S.Y. Dong, J.L. Feng, Y.K. Li et al (2014) Shape-controlled synthesis of BiVO$_4$hierarchical structures with unique natural-sunlight-driven photocatalytic activity, Appl Catal B Environ 152-153:413-424.

[23] Y.Z. Wang, W. Wang, H.Y. Mao (2014) Electrostatic self-assembly of BiVO$_4$-reduced graphene oxide nanocomposites for highly efficient visible light photocatalytic activities, ACS Appl Mater Interfaces 6:12698-12706.

[24] Z.Q. Wang, W.J. Luo, S.C. Yan et al (2011) BiVO$_4$ nano-leaves: Mild synthesis and improved photocatalytic activity for O$_2$production under visible light irradiation, Cryst Eng Comm 13:2500-2504.

[25] F. Li, C.Y. Yang, Q.G. Li, W. Cao, T.H. Li (2011) The pH-controlled morphology transition of BiVO$_4$photocatalysts from microparticles to hollow microspheres, Mater

Lett 145:52-55.

[26] L. Xu, Y.G. Wei, W. Guo et al (2015) One-pot solvothermal preparation and enhanced photocatalytic activity of metallic silver and graphene co-doped $BiVO_4$ternary systems, Appl Surf Sci 332:682.

[27] Z.J. Zhou, M.C. Long, W.M. Cai et al (2012) Synthesis and photocatalytic performance of the efficient visible light photocatalyst Ag-AgCl/$BiVO_4$, J Mol Catal A Chem 353-354:23.

[28] M.C. Long, W.M. Cai, J. Cai et al (2006) Efficient photocatalytic degradation of phenol over Co_3O_4/$BiVO_4$ composite under visible light irradiation, J Phys Chem B 110:20211-20216.

[29] B. Zhou, X. Zhao, H.j. Liu et al (2010) Visible-light sensitive cobalt-doped $BiVO_4$ (Co-$BiVO_4$) photocatalytic composites for the degradation of methylene blue dye in dilute aqueous solutions, Appl Catal B Environ99:214.

[30] J.Q. Li, Z.Y. Guo, H. Liu et al (2013) Two-step hydrothermal process for synthesis of F-doped $BiVO_4$ spheres with enhanced photocatalytic activity, J Alloy Compd 581:40.

[31] Q.M. Wang, Y. Li, Z. Zeng et al (2012) Relationship between crystal structure and luminescent properties of novel red emissive $BiVO_4$:Eu^{3+} and its photocatalytic performance, J Nanopart Res 14:1076.

[32] F. Guo, W.L. Shi, X.Lin, G.B. Che (2014) Hydrothermal synthesis of graphitic

carbon nitride-BiVO$_4$ composites with enhanced visible light photocatalytic activities and the mechanism study, J Phys Chem Solids 75:1217-1222.

[33] L.W. Shan, Y.T. Liu, J. Suriyaprakash et al (2016) Highly efficient photocatalytic activities, band alignment of BiVO$_4$/BiOCl {001} prepared by in situ chemical transformation, J Mol Catal A Chem 411:179.

[34] S.W. Zhu, Q.G. Li, F. Li, W. Cao, T.H. Li(2016) One-pot synthesis of Ag$^+$ doped BiVO$_4$ microspheres with enhanced photocatalytic activity via a facile hydrothermal method, J Phys Chem Solids 92:11-18.

[35] M. Wang, C. Niu, J. Liu (2015) Effective visible light-active nitrogen and samarium co-doped BiVO$_4$ for the degradation of organic pollutants, J Alloy Compd 648:1109-1115.

[36] H.F. Lai, C.C. Chen, Y.K. Chang et al (2014) Efficient photocatalytic degradation of thiobencarb over BiVO$_4$ driven by visible light: Parameter and reaction pathway investigations, Sep Purif Technol 122:80.

[37] T.Y. Zhang, T.i Oyama, S. Horikoshi et al (2002) Photocatalyzed N-demethylation and degradation of methylene blue in titania dispersions exposed to concentrated sunlight, Sol Energ Mat Sol C 73:287-303.

[38] J. Yu and A. Kudo (2016) Effects of structural variation on the photocatalytic performance of hydrothermally synthesized BiVO$_4$, Adv Funct Mater 16:2163-2169.

[39] H. Liu, W.R. Cao, Y. Su et al (2012) Synthesis, characterization and photocatalytic performance of novel visible-light-induced Ag/BiOI, Appl. Catal. B:

Environ 111-112: 271- 279.

[40] S.M. Thalluri, M. Hussain, G. Saracco et al (2014) Green-Synthesized $BiVO_4$oriented along {040} facets for visible-light-driven ethylene degradation, Ind Eng Chem Res 53:2640-2646.

[41] L.X. Wang, J. Zhang, Q.T. Zhang et al (2015) XAFS and XPS studies on site occupation of Sm^{3+} ions in Sm doped M-type $BaFe_{12}O_{19}$, J Magn Magn Mater 377:362-367.

[42] A.P. Zhang, J.Z. Zhang (2009) Synthesis and activities of Ln-doped $BiVO_4$ (Ln=Eu,Gd and Er) photocatalysts, Chinese J Inorg Chem 25:2040-2047.